

Disentangling transients and their host galaxies with SCARLET2: A framework to forward model multi-epoch imaging

Charlotte Ward^{①a}, Peter Melchior^{①a,b}, Matt L. Sampson^{②a}, Colin J. Burke^{③c}, Jared Siegel^{②a}, Benjamin Remy^{④a},
Sufia Birmingham^{②a}, Emily Ramey^{②d}, Sjoert van Velzen^{④e}

^aDepartment of Astrophysical Sciences, Princeton University, Princeton, 08544, NJ, USA

^bCenter for Statistics and Machine Learning, Princeton University, Princeton, 08544, NJ, USA

^cDepartment of Astronomy, Yale University, 266 Whitney Avenue, New Haven, 06511, CT, USA

^dDepartment of Astronomy, University of California, Berkeley, Berkeley, 94720, CA, USA

^eLeiden Observatory, Leiden University, Postbus 9513, 2300 RA, Leiden, the Netherlands

Abstract

Many science cases for wide-field time-domain surveys rely on accurate identification and characterization of the galaxies hosting transient and variable objects. In the era of the Legacy Survey of Space and Time (LSST) at the Vera C. Rubin Observatory the number of known transient and variable sources will grow by orders of magnitude, and many of these sources will be blended with their host galaxies and neighboring galaxies. A diverse range of applications – including the classification of nuclear and non-nuclear sources, identification of potential host galaxies in deep fields, extraction of host galaxy SEDs without requiring a transient-free reference image, and combined analysis of photometry from multiple surveys – will benefit from a flexible framework to model time-domain imaging of transients. We describe a time-domain extension of the SCARLET2 scene modeling code for multi-epoch, multi-band, and multi-resolution imaging data to extract simultaneous transient and host galaxy models. SCARLET2 leverages the benefits of data-driven priors on galaxy morphology, is fully GPU compatible, and can jointly model multi-resolution data from ground and space-based surveys. We demonstrate the method on simulated LSST-like supernova imaging, low-resolution Zwicky Transient Facility imaging of tidal disruption events, and Hyper Suprime Cam imaging of variable AGN out to $z = 4$ in the COSMOS fields. We show that SCARLET2 models provide accurate transient and host galaxy models as well as accurate measurement of host–transient spatial offsets, and demonstrate future applications to the search for ‘wandering’ massive black holes.

Keywords: methods: data analysis, machine learning, techniques: image processing

1. Introduction

The next generation of wide-field optical time-domain surveys such as the Legacy Survey of Space and Time at Vera C. Rubin observatory (LSST; [Ivezic et al., 2008](#)) and the High Latitude Time Domain Survey planned for the *Nancy Grace Roman Space Telescope* (*Roman*; [Akeson et al., 2019](#)) will provide enormous discovery potential for high-redshift and low-luminosity transient phenomena such as supernovae (SNe), tidal disruption events (TDEs), and gamma ray burst (GRB) afterglows. Prompt classification of transient and variable objects – essential to various extragalactic science

cases where fast spectroscopic follow-up is particularly informative – depends on our ability to correctly identify the host galaxies of transients, measure the distance between transients and their host galaxy nuclei, and estimate photometric redshifts from the host galaxy spectral energy distributions (SEDs). This becomes particularly challenging at the depths of LSST, where 30–50% of galaxies in single epoch LSST images will overlap other galaxies, and 15% of sources will be blended with other sources without being recognized as such ([Melchior et al., 2021](#)).

Time-domain surveys frequently employ methods based on a technique called ‘difference imaging’ to detect transient phenomena. In such an approach, a deep ‘reference image’ is produced from a stack of high quality images and subtracted from new images to produce a

Email address: charlotte.ward@princeton.edu (Charlotte Ward^②)

difference image (Alard and Lupton, 1998). Difference imaging enables the efficient detection and optimal extraction of multi-epoch fluxes of transient sources. In this work, we are primarily concerned with enabling follow-up investigations of the transient and its host once the transient has been identified by difference imaging. We propose a model of a variable point source *and* a non-varying host galaxy that is rendered to match all observations. Our approach is particularly advantageous when the difference imaging introduces ambiguities – for example, when the variable object is already contributing to the reference image, which is always the case for AGNs – or when simultaneously modeling the transient and the host is helpful, such as when measuring small spatial offsets between the host center and the transient. Our approach can also make use of imaging data from different surveys, enabling the automatic production of combined light curves without concerns about mismatches between the reference image epochs.

Multi-resolution scene modeling methods have previously been applied to produce galaxy catalogs from deep stacks for the DESI Legacy Imaging Surveys (Dey et al., 2019), and to produce deep forced photometry of 400 million sources in low resolution imaging from the *Wide-Field Infrared Survey Explorer*, exploiting higher resolution SDSS imaging to anchor the photometry (Lang et al., 2016). However, scene modeling has rarely been implemented for multi-epoch imaging of transients. A version of the scene modeling approach was applied to produce supernova photometry in the Sloan Digital Sky Survey-II Supernova survey (Holtzman et al., 2008) and the Dark Energy Survey Supernova Program survey (Brout et al., 2019), but is yet to be applied at scale for nuclear transients and AGN.

Scene modeling is particularly powerful when imaging data from ground and space-based telescopes is combined so that the high-resolution imaging with small PSF sizes can improve galaxy deblending solutions for sources that are marginally resolved in low-resolution ground-based imaging (Melchior et al., 2021). Software packages that can simultaneously model multi-band, multi-resolution imaging data include THE TRACTOR (Lang et al., 2016), SCARLET (Melchior et al., 2018), and ASTROPHOT (Stone et al., 2023), the latter of which is GPU-accelerated. In contrast to THE TRACTOR and ASTROPHOT, SCARLET is a non-parametric method: it does not require the adoption of an analytical profile such as a Sérsic profile for extended sources. Simple requirements on galaxy shape, such as a monotonically decreasing or symmetric profile, or positive flux in all regions of the galaxy, are enforced by proximal operators. Gradient descent with Autograd

is used to fit the source parameters, with the differing colors of overlapping sources being the most important distinguishing factor for deblending.

Recently, a new version of SCARLET was introduced (Sampson et al. (2024); Melchior et al., in prep.). SCARLET2 is built with jax (Bradbury et al., 2018) and equinox (Kidger and Garcia, 2021) for CPU/GPU compatibility. Importantly, SCARLET2 has the ability to utilize data-driven priors for galaxy morphologies in the form of score-based neural networks, which replace the hard physical constraints placed on the morphology models in SCARLET. The galaxy morphology priors significantly stabilize non-parametric model fitting of low-S/N and highly blended sources. In the context of this work, flexible galaxy models are essential for producing transient photometry via scene modeling, as the enforcement of a parametric galaxy profile that does not fully describe the data will generate seeing-dependent errors on the measured transient flux. SCARLET2 also supports numpyro (Phan et al., 2019; Bingham et al., 2019) to undertake MCMC sampling over source parameters to enable careful quantification of uncertainties in source positions, SEDs and morphologies. The combination of GPU acceleration for fast fitting, MCMC sampling, and the capacity to fit non-parametric galaxy models makes SCARLET2 a capable base for a wide range of scene-fitting applications.

In this paper, we introduce a new time-domain extension to SCARLET2 that enables modeling of multi-band, multi-resolution *and* multi-epoch imaging data, where we treat some sources to as variable and others as static. We test the methodology on simulated multi-epoch, multi-band supernova imaging, and then demonstrate it on real survey data for samples of a) TDEs and b) AGNs. For our two case studies, we apply our scene-modeling technique to a) high cadence, low resolution, shallow multi-epoch imaging from the Zwicky Transient Facility (ZTF; Graham et al., 2019; Bellm et al., 2019; Dekany et al., 2020) and b) low cadence, high resolution, deep multi-epoch imaging from the Hyper Suprime Cam Subaru Strategic Program (HSC-SSP) Transient Survey (Yasuda et al., 2019). We demonstrate the application of non-parametric galaxy morphology models, guided by data-driven neural network priors, to produce full scene models with accurate transient photometry and position measurements.

2. Modeling variable and static sources in multi-epoch imaging

In SCARLET, a multi-band image cube \mathbf{Y} is described as the linear combination of K sources, each of which

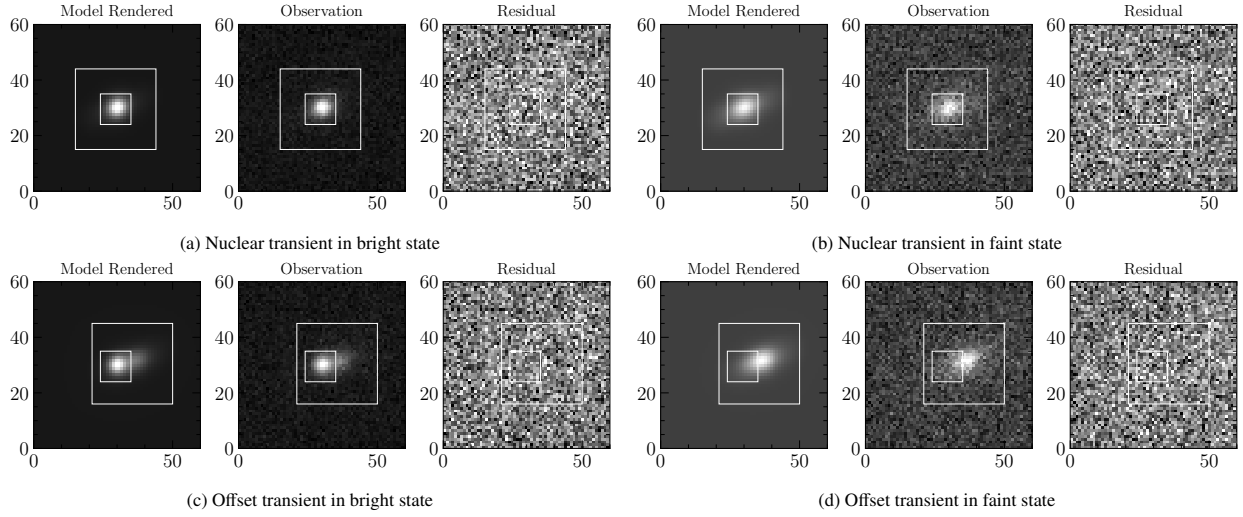


Figure 1: Example of a simulated supernova and host galaxy system and the resulting SCARLET2 models for two different host-transient spatial offsets. SCARLET2 models were derived from simulated imaging with a 0.17" pixel scale over 10 epochs and 3 bands (g , r , and i). *Top*: A transient coincident with the galaxy nucleus while it is bright relative to the host galaxy (left) and faint relative to the host galaxy (right). *Bottom*: Same as above but for a transient offset by 1.06".

with its own amplitude \mathbf{A}_k and intensity variation (morphology) \mathbf{S}_k :

$$\mathbf{Y} = \sum_k^K \mathbf{A}_k \times \mathbf{S}_k. \quad (1)$$

The amplitude vector $\mathbf{A}_k \in \mathbb{R}^B$ has dimension equal to the number of different bands B and contains the source spectrum or SED. The source morphology image $\mathbf{S}_k \in \mathbb{R}^{H \times W}$ has a size given by the height and width of either the observations \mathbf{Y} or the area of the sky we seek to model. This construction allows each source to have a free-form morphology that is constant across bands up to a multiplicative amplitude rescaling.

We now extend this definition for time-domain models, by generalizing $\mathbf{A}_k \in \mathbb{R}^E$ to contain the amplitudes for the total number of observed images E , which can be different in wavelength *and in time*. We assume to know the presence of static sources from regular source detection, and of variable sources from difference imaging, and we use this information to create a scene containing variable sources (which are allowed to change in flux across epochs) and ‘static’ sources (which must not change their spectrum across epochs). For the former, the amplitude is independent across all epochs:

$$\mathbf{A}_k^{\text{variable}} = \{A_{k,e} \text{ for } e \in E\}. \quad (2)$$

For the latter, we construct the full amplitude vector

$$\mathbf{A}_k^{\text{static}} = \{\bar{A}_{k,b(e)} \text{ for } e \in E\} \quad (3)$$

from a time-independent SED vector $\bar{\mathbf{A}}_k \in \mathbb{R}^B$, where $b(e)$ refers to the band used for exposure e .

We also enable the user to optionally incorporate information about the exposures E_{on} when the transient is present and may therefore have a non-zero flux and model the transient amplitude as

$$\mathbf{A}_{k,e}^{\text{variable}} = \begin{cases} A_{k,e} & \text{if } e \in E_{\text{on}} \\ 0 & \text{else.} \end{cases} \quad (4)$$

By providing SCARLET2 with information about the epoch and band of each image, and then defining sources as having either a variable or a static spectrum, a scene model with both varying and unvarying sources may be fit across multi-band, multi-epoch imaging data. Additional information about when a transient is ‘on’ or ‘off’ can be used as an additional constraint for transients with pre- or post-flare imaging, helping images from the transient-free epochs to improve the host galaxy SED and morphology model.

3. Photometric and astrometric quality in simulated supernova imaging

With the extension from section 2, SCARLET2 can produce light curves and measure transient–host spatial offsets for a suite of simulated supernovae in LSST-like multi-epoch imaging. To produce the multi-epoch images, we first used SNCosmo (Barbary et al., 2016) to

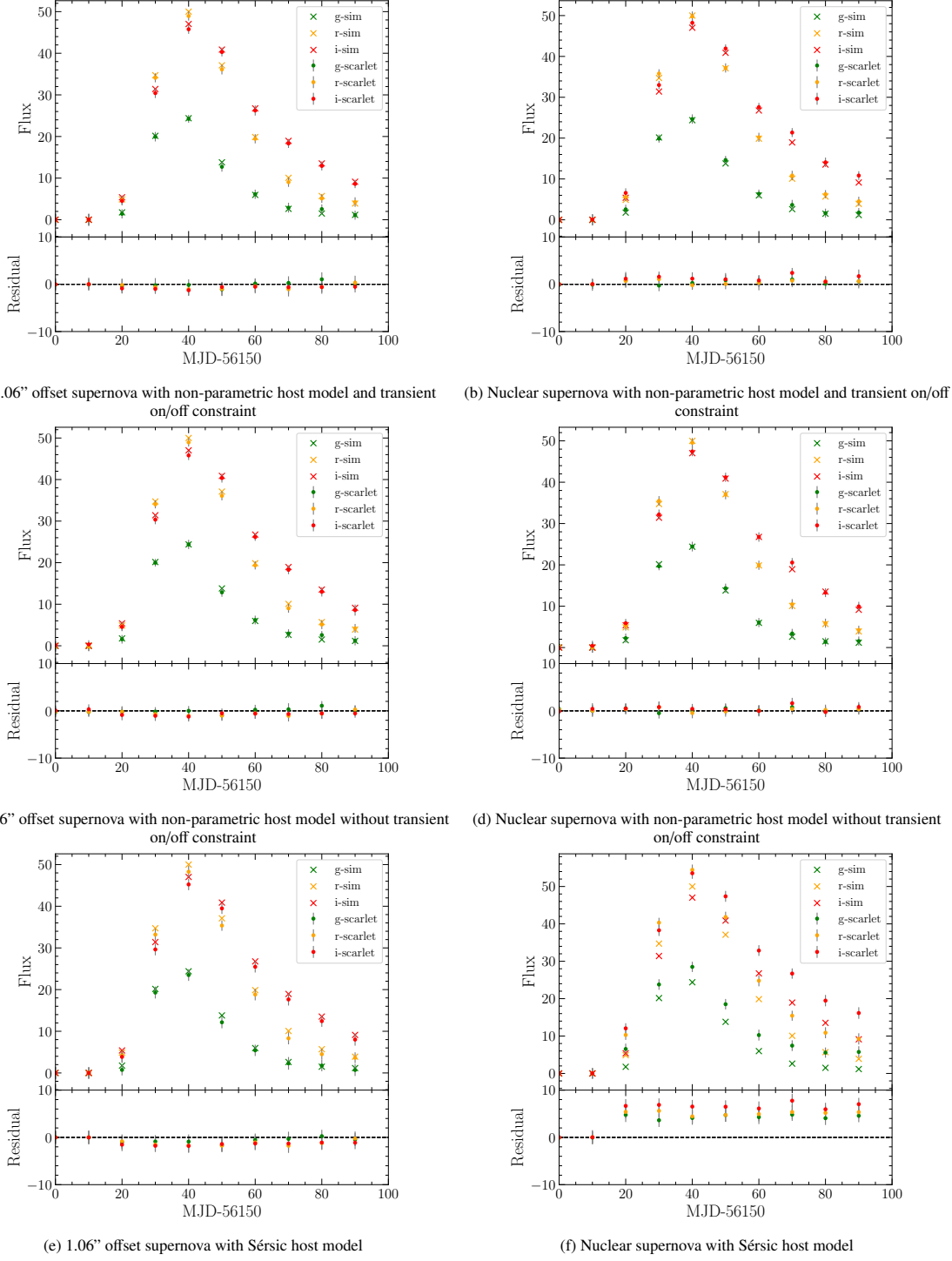


Figure 2: SCARLET2 light curves compared to simulated values for a supernova located 1.06'' from the galaxy nucleus (left) and in the galaxy nucleus (right). We show 3σ uncertainties from the posterior derived from MCMC sampling over the supernova flux and position, and host galaxy SED and morphology. We show results from modeling with three different constraints: A non-parametric host galaxy model with a transient that is constrained as ‘on’ during the supernova and ‘off’ otherwise (top row), a non-parametric host galaxy model with a transient that has no on/off constraint applied (middle row), and a Sérsic host model with a transient that has the on/off constraint applied (bottom row). The flexible non-parametric morphology model does not impose an analytical profile onto realistic galaxies that may introduce biases in the transient photometry.

simulate the multi-band light curve of an SNIa at redshift $z = 0.4$, generating g , r and i band fluxes for 15 epochs over a period of 240 days beginning 100 days before the onset of the supernova. We used `galsim` (Rowe et al., 2015) to simulate realistic images of the supernova and its host galaxy. We generated two sets of simulated images: one for an extended host galaxy with a bulge radius of $0.8''$ and a disk radius of $1.8''$, and one for a compact host galaxy with a bulge radius of $0.3''$ and a disk radius of $0.5''$. In each case the galaxy axis ratio was set to 0.43 and the position angle to 23 degrees. Images of size 65 by 65 pixels, with a pixel scale of $0.17''/\text{pixel}$, a PSF FWHM of $0.8''$, and a sky noise level of 10 ADU per arcsec^2 , were generated for each band and epoch. We generated the set of 45 multi-band, multi-epoch images for a series of spatial offsets between the supernova and the host center: $0.0'', 0.03'', 0.07'', 0.14'', 0.28'', 0.49'', 0.71'', 1.06'', 1.41'',$ and $2.12''$.

To generate SCARLET2 scene models of the simulated supernova images, we first ran the wavelet detection routine implemented in SCARLET (Melchior et al., 2018) on the summed images using the first 3 wavelet levels. If a single source was detected, we initialized the SCARLET2 model with a point source and a single extended source at the position found by the detection routine. If the detection routine found 2 sources (which was the case for offsets $> 0.5''$), we initialized the point source and extended source models at the best-fit positions found by the detection routine.

The extended sources were modeled with the non-parametric `Source` class, with initial morphologies taken from an elliptical Gaussian fit to the summed image and a `StaticArraySpectrum`, following Equation 3, with initial values obtained from the peak pixel. The `Source` morphology was given the positive constraint and the `ZTF_ScoreNet32` prior from the score-model of the `galaxygrad`¹ package (Sampson et al., 2024). This model was trained to match the distributions of extended source galaxies in ZTF, which will match the host properties of our simulations well overall but lack finer detail.

The SNe are modeled as `PointSource` objects, i.e. their morphology is identical to the PSF. Their spectra were either complete free `ArraySpectrum`, following Equation 2, or `TransientArraySpectrum`, following Equation 4, depending on whether the transient on/off constraints were being tested, with initial values taken from the pixel associated with their detection location.

¹<https://github.com/SampsonML/galaxygrad>

SCARLET2 then fit the scene until a relative error of 10^{-6} was reached, or a maximum of 3000 steps.

After obtaining the scene model, we used the `numpyro` NUTS MCMC sampling routine (Phan et al., 2019; Bingham et al., 2019) implemented within SCARLET2 to sample over the point source position, the host galaxy spectrum, and the supernova flux in each epoch and estimate their uncertainties. For this exploratory study, we set a Gaussian prior of width given by 10% of the best-fit value for each parameter. We ran the MCMC sampler for 200 burn-in iterations and 500 sampling iterations.

In Figure 1 we show observations, rendered models, and residuals based on the results of the full multi-epoch scene model for one g -band image when the supernova is bright and one pre-flare image. We distinguish two cases: In the top row, the supernova is located at the center of the galaxy nucleus; in the bottom row, it has a $1.06''$ offset from the galaxy nucleus. By modeling the full sets of 45 images with a variable point source and static host galaxy, SCARLET2 is able to produce accurate scene models for all single-epoch images. In Figure 2 we show the best-fit SCARLET2 point-source flux for each epoch vs the true simulated flux. SCARLET2 provides accurate photometry for all simulated supernovae, even when the supernova is coincident with the galaxy nucleus. We show light curves for simulated supernova imaging obtained both with and without the transient on/off constraint, and find that the inclusion of pre-supernova imaging is sufficient to accurately decompose the supernova and galaxy flux, regardless of whether the constraint is applied.

In Figure 2, we also compare the quality of the transient photometry derived when using a non-parametric galaxy morphology model to an alternative approach where SCARLET2 is required to fit a Sérsic galaxy model, with free parameters for the central position, ellipticity, half-light radius, and Sérsic index describing the steepness of the profile. As the selected parametric model cannot fully describe the simulated disk and bulge galaxy profiles, the galaxy flux is underestimated in the center and overestimated in the outskirts, producing underestimated transient fluxes for the spatially offset supernova and overestimated transient fluxes for the nuclear supernova. While a more complex multi-component parametric model could improve the transient photometry in this case, the non-parametric model provides a flexible approach that enables accurate transient photometry without careful selection of the best parametric model.

In order to calculate the spatial offsets between the simulated supernovae and their host galaxy, we first

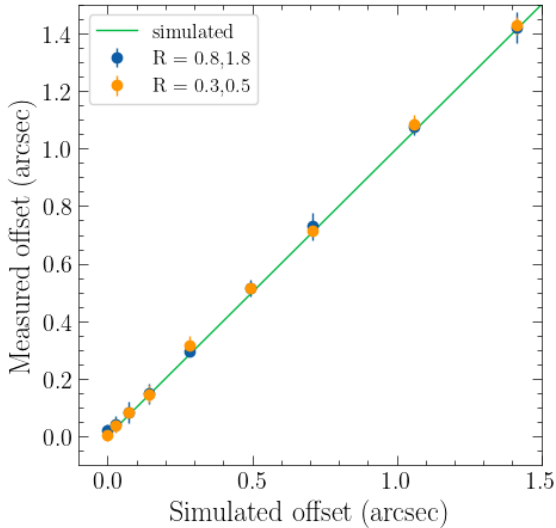


Figure 3: Measured transient-host spatial offsets from simulated imaging of a transient at various distances from the nucleus of its host galaxy. We show the results for two host galaxies of different sizes: one with bulge radius of $0.8''$ and disk radius of $1.8''$ (corresponding to the images in Figure 1) shown in blue, and another with a bulge radius of $0.3''$ and disk radius of $0.5''$ shown in orange. Uncertainties are 1σ uncertainties derived from the posterior that was obtained when sampling over the source parameters.

needed to determine the center of the galaxy nucleus to sub-pixel accuracy. To do this, we first prepared a high S/N galaxy image by subtracting the rendered SCARLET2 model of the transient from each observation, and then stacking those transient-subtracted multi-epoch images to produce a high S/N multi-band image of the host galaxy. We then fit a Sérsic galaxy model to the transient-subtracted image to fit the center of the galaxy by initializing a Sérsic profile and allowing SCARLET2 to fit the half light radius, ellipticity, Sérsic index, spectrum, and central position. The MCMC sampling routine was again applied to determine the uncertainties for the galaxy model parameters. The offset between the best-fit point source position derived from the original non-parametric scene model and the best-fit galaxy center from the Sérsic profile fit to the transient-subtracted image stack was calculated for each set of simulated images. In Figure 3 we show the best-fit spatial offsets found by the SCARLET2 fits vs the known simulated offset for the compact galaxy profile and the extended galaxy profile. Our fitting routine is able to correctly measure both small and large spatial offsets between supernovae and their host galaxies, for both extended and compact host morphologies.

4. Tidal disruption events in low-resolution Zwicky Transient Facility imaging

4.1. Background and motivation

We extend our study to much lower resolution images and demonstrate how to use SCARLET2 to measure transient-host offsets and produce accurate photometry of low redshift transients in galaxy nuclei using the sample of 17 TDEs discovered in ZTF-I (van Velzen et al., 2021). In the ZTF survey, measuring the distance between transients and their host nuclei was challenging given the $1.0''$ pixel scales. The ‘nuclear transient alert filter’ for ZTF, which was designed to use difference imaging metadata to identify TDEs and AGN flares, required that the mean spatial offset between the position of the transient in all difference images containing detections and the centroid of the closest source in the reference image be less than $0.4''$ (van Velzen et al., 2021). However, the distribution of spatial offsets measured for nuclear AGN via this method was shown to extend to $\lesssim 0.95''$ (Ward et al., 2021). In one case, the optical counterpart to an X-ray identified TDE had an overestimated transient-host offset based on ZTF difference imaging statistics such that it did not meet the $< 0.4''$ cutoff, and a full scene model of the point source and host galaxy in the ZTF imaging was required to ascertain that the optical transient seen in ZTF was indeed coincident with the galaxy nucleus and therefore associated with the X-ray TDE (Brightman et al., 2021).

4.2. Light curves, host galaxy morphology models, and spatial offsets for ZTF TDEs

To produce SCARLET2 light curves and host galaxy models of the ZTF-I TDEs, we first used the ZTFquery cutout service (Rigault, 2018) to download $120''$ by $120''$ cutouts of the ZTF single-epoch imaging of each TDE. We obtained imaging covering 900 days, beginning from 50 days prior to the TDE, and removed images with seeing $\text{FWHM} > 2''$ and limiting magnitude < 20 . This resulted in approximately 300 g , r and i band images per scene. We repeated the procedure described for the simulated galsim imaging in section 3, running SCARLET2 with the 32 by 32 pixel ZTF prior to produce non-parametric models of each host galaxy and blended background galaxies, in addition to a variable point source initialized at the galaxy center. Example ZTF images and models of two TDEs are shown in Figure 4.

After obtaining a full scene model, including the single-epoch fluxes for the transient, we again produced a stack of the transient-subtracted single-epoch images to fit a Sérsic model to a high S/N host galaxy image

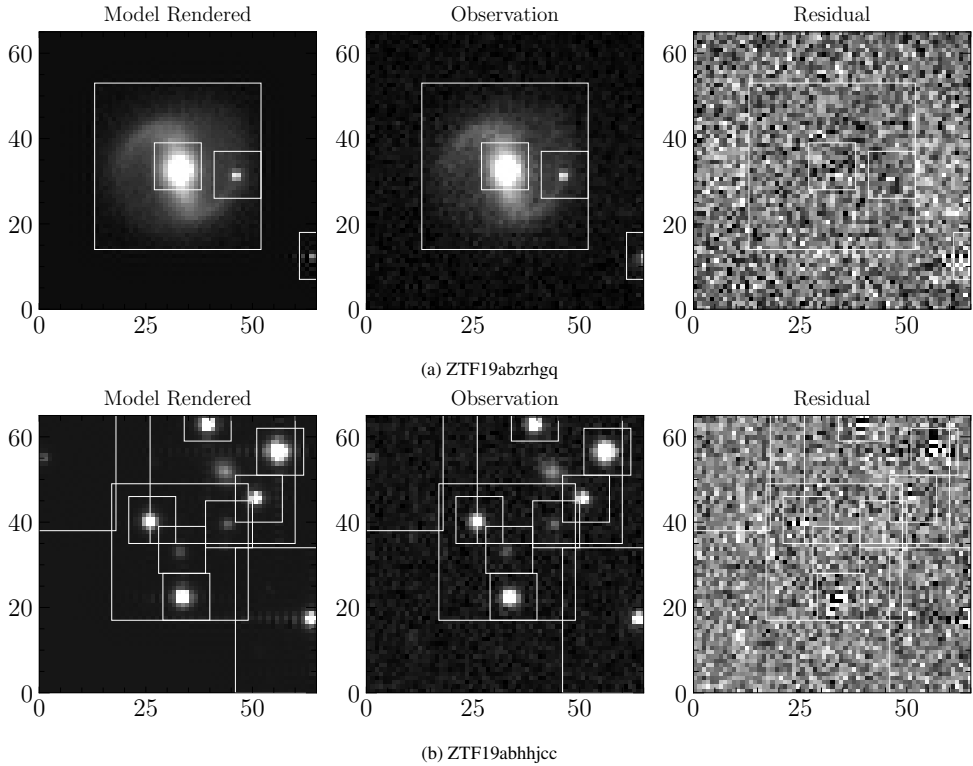


Figure 4: Example SCARLET2 rendered models, observations, and residuals produced by modeling the full multi-epoch, multi-band ZTF imaging dataset for two TDEs. We show a TDE with a large and complex host galaxy above and a TDE with a compact host galaxy in a busy field below. Some artifacts due to the undersampled PSF are visible.

to measure the center of the galaxy nucleus. From the MCMC sampling results, we find that all TDEs are consistent with the galaxy nuclei as expected, with all best-fit offsets $< 0.9''$. Typical 3σ spatial offset uncertainties reported from MCMC sampling over source SEDs, positions, and morphologies were $1\text{--}2''$, consistent with previous analysis of the spatial offset uncertainty distribution of variable AGN reported from ZTF difference imaging (Ward et al., 2021).

In Figure 5 we show the the single-epoch fluxes measured by SCARLET2 for one of the ZTF TDEs, ZTF19abhhjc, as well as the equivalent light curve produced using the forced photometry pipeline for ZTF difference imaging (Masci et al., 2019). SCARLET2 is able to produce a light curve consistent with the difference imaging pipeline, and correctly assigns flux to the host galaxy and the nuclear transient where they are blended. We specifically chose ZTF19abhhjc because it represents a more difficult modeling problem: the host galaxy is compact (Figure 4), such that there is little extended emission beyond the nucleus to assist in decomposing the nuclear transient and host galaxy SEDs.

In Figure 6, we show the non-parametric galaxy mor-

phology models for 8 of the TDE host galaxies. The galaxy morphology models are able to describe complex shapes including spiral arms. By using a non-parametric model for the host galaxy and background galaxies we are able to produce high quality light curves that are not contaminated by residuals in the galaxy model, which can arise when enforcing a simplified parametric galaxy model.

In summary, SCARLET2 scene modeling can correctly extract transient photometry, galaxy morphology models, and transient-host spatial offsets for our test sample of nuclear transients even in low-resolution ZTF imaging. Sampling over source parameters enables accurate quantification of transient–host spatial offsets and source SEDs. SCARLET2 can therefore be applied to large multi-epoch datasets to confirm whether TDEs and TDE candidates are coincident with galaxy nuclei.

5. Variable AGN in the HSC-SSP Transient Survey

5.1. Background and motivation

The HSC-SSP transient survey was a high-resolution, narrow-field, deep survey, with $0.17''$ pixel scales and

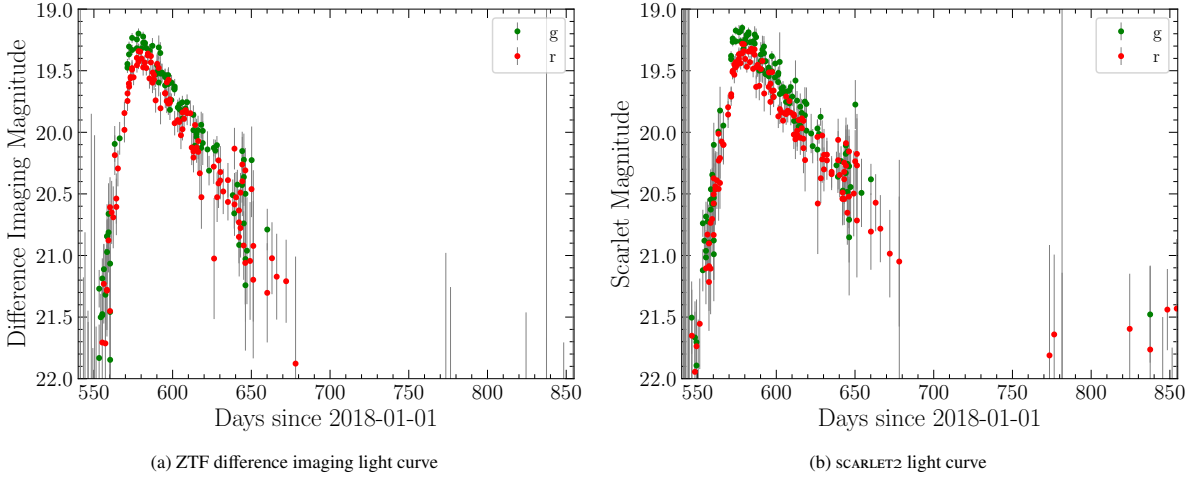


Figure 5: Comparison of light curves of example TDE ZTF19abhhjc produced by forced photometry on ZTF difference imaging (left) and SCARLET2 scene modeling (right).

single-epoch depths of $g \sim 26.4$ in the 1.77 square degree ultra-deep fields, which were surveyed in g , r , i , z and y bands (Aihara et al., 2022). At these depths, an estimated 60% of sources were blended (Bosch et al., 2018). We now apply our scene-modeling approach to the characterization of variable AGN in deep multi-epoch imaging from the HSC-SSP transient survey.

AGN studies are a key science driver for LSST, which is expected to observe on the order of 10 million AGN (De Cicco et al., 2021; Bianco et al., 2022). A large fraction of Type 1 AGNs are variable: at least 90% of Stripe-82 quasars of magnitude $g < 20.5$ exhibit variability greater than 0.03 mags (Sesar et al., 2007; Barth et al., 2014). Variability selection is therefore a key tool for quasar identification (MacLeod et al., 2011; Butler and Bloom, 2011, e.g) and has been found to produce major improvements in classification completeness compared to techniques based on color and morphology criteria alone in simulated LSST data (Palanque-Delabrouille et al., 2011; Savic et al., 2023; Burke et al., 2023). Though variability enables highly complete AGN sample selection, optically variable AGN will also be a major source of contamination in searches for other transients: in the ZTF TDE alert filter, for example, mid-IR variability in the WISE survey was essential for removing AGN contaminants (van Velzen et al., 2021). The presence of a bright and variable AGN can inhibit accurate extraction host galaxy SEDs, and therefore the estimation of photometric redshifts, which are important not only for cosmology studies but for identifying the hosts of transients such as GRBs and kilonovae (Nugent et al., 2022).

As part of our HSC AGN analysis, we undertake a pilot study for the search for rare MBHs that are spatially offset from their host galaxy nuclei, in preparation for a larger-scale analysis with LSST. Recent cosmological simulations that do not artificially tie SMBHs to halo centers have found that the majority of SMBHs of mass $M_{\text{BH}} < 10^7 M_{\odot}$ have a $> 15\text{kpc}$ spatial offset from their host nucleus, with the fraction increasing for decreasing mass (Bellovary et al., 2019; Ricarte et al., 2021). Variability-selection has proven to be particularly effective at identifying low mass AGN in dwarf galaxies where traditional spectroscopic diagnostics are less effective (e.g. Baldassare et al., 2018, 2020; Ward et al., 2022; Burke et al., 2022), making it a promising approach for the identification of wandering MBHs. Forecasts for the number of $10^4 M_{\odot} < M_{\text{BH}} < 10^6 M_{\odot}$ MBHs with detectable variability in LSST range from 1,500 to 21,000 depending on seed mass and wandering fraction (Burke et al., 2023).

There are a variety of predictions for the accretion luminosities of such wandering AGN (Pacucci et al., 2018; Di Matteo et al., 2023), but even if they are not observable from typical gas accretion, they may be observable as tidal disruption events if the wandering SMBHs retain their nuclear star clusters (e.g Lin et al., 2018). The goal of this pilot study is to determine what spatial offsets will be detectable by applying multi-epoch scene modeling to LSST-like imaging data, using a sample of variable AGNs with well-determined spectroscopic redshifts and black hole masses (Aihara et al., 2022; Burke et al., 2024).

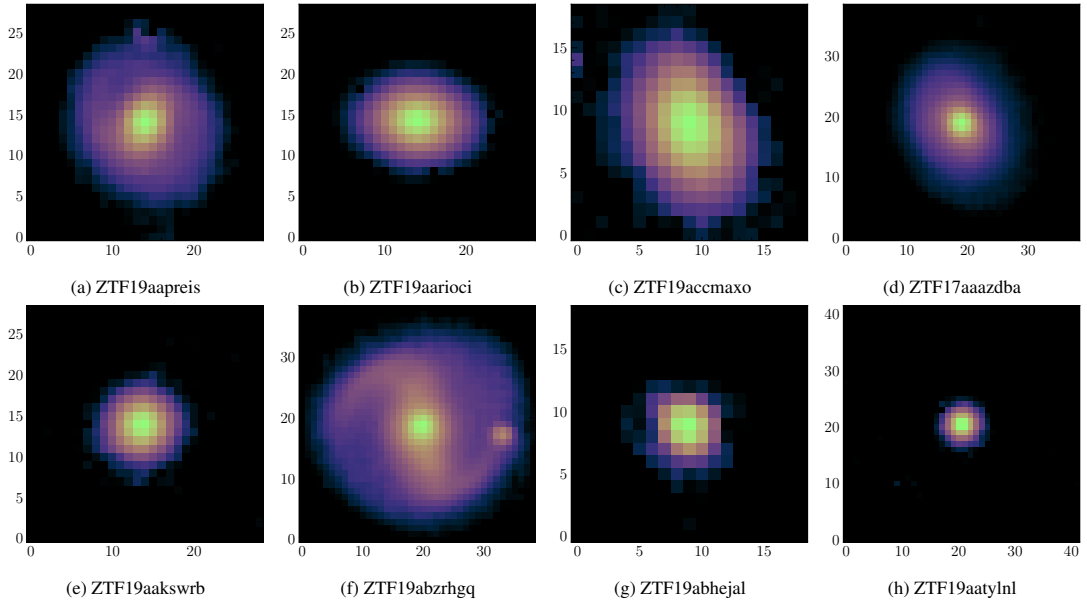


Figure 6: Example SCARLET2 morphology models for 8 TDE host galaxies in ZTF imaging, shown with logarithmic scaling. The non-parametric modeling approach, guided by the custom ZTF prior, enables accurate descriptions of asymmetric and non-monotonically decreasing galaxy morphologies (e.g. ZTF19aapreis and ZTF19abzrhgq).

5.2. Light curves, host galaxy SEDs, and spatial offset distributions for variable AGN in HSC

In this section we will analyze 542 variable AGN in the Hyper Suprime Cam imaging of the $\sim 1.5 \text{ deg}^2$ COSMOS-field (Aihara et al., 2022) without the need for reference images. A previous spectroscopic study of this sample found these AGNs to have redshifts up to $z \sim 4$ and employed SED fitting to determine that the host galaxy stellar masses fell between $10^{8.5} M_\odot < M_* < 10^{11}$; the BH mass distribution of this sample spans the range of $10^7 M_\odot < M_* < 10^{9.8}$ (Burke et al., 2024).

We used the HSC data-access-tools to obtain 120×120 arcsec cutouts of the multi-epoch warped (aligned and sky subtracted) HSC images and corresponding PSF images from the deep and ultra-deep fields in the Public HSC Data Release 3 (Aihara et al., 2022). We obtained approximately 100 *grizy* images for each AGN. We repeated the SCARLET2 modeling procedure described for the ZTF TDEs in section 3 with two major differences. Firstly, we did not apply any constraints on whether the transient is ‘on’ or ‘off’ because the variable AGN are always present to some extent. Secondly, because our primary motivation was the measurement of transient–host nucleus offsets and the host galaxies were very compact and faint, we instead enforced a Sérsic profile for the initial scene models, rather than applying a non-parametric galaxy model then fitting a Sérsic profile to the transient-subtracted image.

In Figure 7, we show a HSC observation, the SCARLET2 model for that observation derived from fitting the full multi-epoch data set, and the corresponding residual image for two COSMOS AGN: one in a compact, AGN-dominated galaxy – which is very typical for this sample – and one in an extended galaxy of comparable flux to the variable AGN. SCARLET2 produces high quality models and light curves for all AGN in the HSC sample. Three example light curves from this procedure are shown in Figure 8.

In Figure 9, we compare the host galaxy SED from the SCARLET2 model with the estimated host galaxy SED from a spectroscopic decomposition of the combined AGN and host spectrum obtained from *cigale* (Boquien et al., 2019) fitting, as reported in Burke et al. (2024). We show the results for a host galaxy-dominated system and an AGN-dominated system. SCARLET2 finds comparable galaxy SEDs to the *cigale* model results, even when only presented with *grizy* images. In addition, the SCARLET2 sampling procedure enables the quantification of uncertainties in the galaxy SED arising from the presence of the AGN.

We point out that in this comparison the *cigale* model may not be able to establish the ground truth for the host spectrum either. However, the imaging-based decomposition we performed with SCARLET2 suffers from a different set of degeneracies. For extremely compact and high redshift galaxies, i.e. with insuffi-

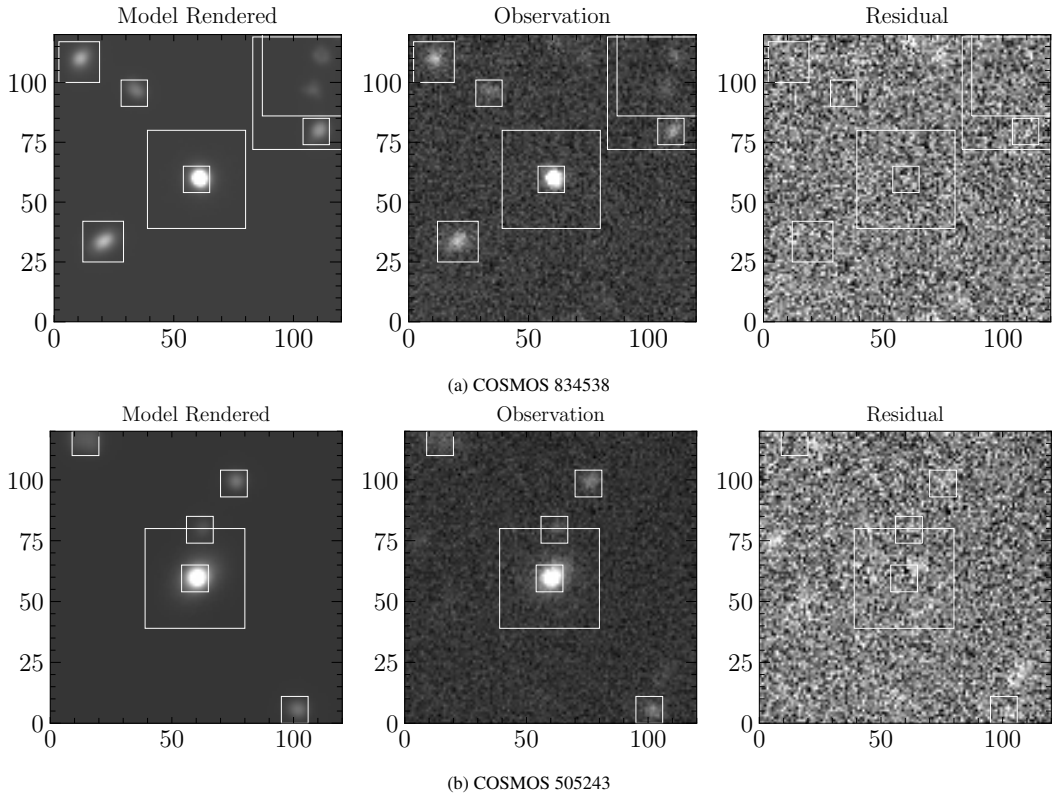


Figure 7: Example SCARLET2 models and residuals for single exposures based on modeling of the full multi-epoch, multi-band HSC imaging dataset for two variable COSMOS AGN. We show an AGN with a compact, faint host galaxy above and an AGN with faint but extended host galaxy emission below.

cient extended emission from the galaxy to determine its SED from regions uncontaminated by the AGN, the AGN spectrum and host galaxy spectrum cannot be separated without additional assumptions—which `cigale` makes, but we have not. In such cases, SCARLET2 can produce light curves that accurately represent the variability, but cannot decide to which object it should attribute the minimum flux level of both sources. In such cases, including a single high-resolution space-based image with a more compact PSF would enable SCARLET2 to better distinguish between the host galaxy emission and the nuclear AGN emission because the AGN’s effective area of influence is smaller. Future work will investigate the incorporation of existing Hubble Space Telescope imaging of the COSMOS AGN (Zhong et al., 2022) into SCARLET2 modeling for improved AGN-host decomposition. We will also investigate the option for spectral priors to aid this decomposition.

Our method can be applied to identify the presence of spatially offset ‘wandering’ AGN in future LSST imaging. The distribution of host–AGN offsets (Figure 10) peaks at around a quarter of a pixel, and is well-fit by

a mixture distribution consisting of a Rayleigh distribution (expected for a population of offsets given some typical positional uncertainty) with $\sigma = 0.051''$ and an exponential tail with exponent $\alpha = 14.2$. The ratio between the two components of the mixture distribution was 1:0.56. In Figure 11 we show the probability that an offset greater than R is drawn from the Rayleigh component of the mixture distribution shown in Figure 10 instead of the exponential component. We find that our modeling strategy applied to LSST-like imaging will be sensitive to spatial offsets $> 0.22''$ when applying a 3σ cutoff. Such objects should be investigated as potential candidates for spatially offset AGN. This distribution and offset cutoff is much smaller than that measured from the ZTF AGN sample, which was limited by the low resolution 1.0'' pixel scale (Ward et al., 2021). As a result, in future work with larger AGN populations, differences in offset as a function of MBH mass could be compared to predictions of wandering fraction vs mass from cosmological simulations, where the majority of MBHs of mass $10^8 M_\odot$ are expected to be non-nuclear.

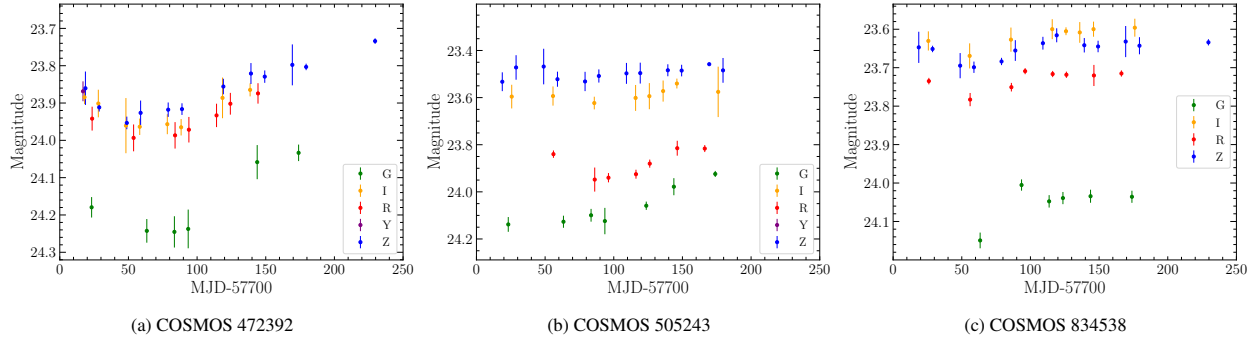


Figure 8: Example SCARLET2 light curves of the AGN in the HSC-SSP transient survey, zoomed into a 250 day period with high cadence monitoring. Long term AGN variability at the ~ 0.1 magnitude level consistent across 3 to 5 HSC bands is detected for all AGN in the sample.

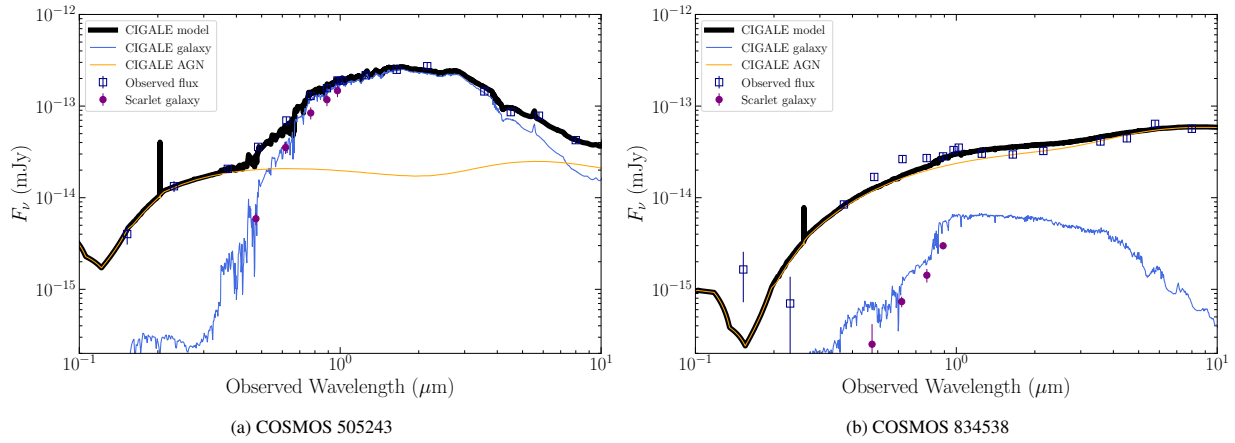


Figure 9: Comparison of galaxy and AGN SEDs estimated from `cigale` modeling of combined host and AGN spectra and those estimated from multi-band, multi-epoch HSC imaging modeling with SCARLET2. The observed fluxes derived from an optical spectrum are shown in blue boxes. The total `cigale` model derived from the fluxes is shown in black. The AGN contribution to the model is shown in orange and the host galaxy's stellar contribution in blue. Overlaid onto the `cigale` results are the best-fit scarlet SEDs for the host galaxy with 1σ uncertainties derived from scene modeling of multi-epoch HSC imaging. We show the results for two galaxies: one where the `cigale` model estimates a substantial contribution from the host galaxy to the total flux in the wavelength range of the HSC imaging (left) and one where the `cigale` model estimates that the stellar component is dominated by the AGN component in the wavelength range of the HSC imaging (right). In both cases SCARLET2 finds results comparable to the spectroscopic decomposition via imaging modeling alone.

6. Summary and conclusions

We have presented a time-domain extension to the SCARLET2 scene modeling and deblending code. It can model multi-epoch, multi-band, multi-resolution imaging data without the need for reference or difference images and constrain source fluxes as either time-varying or ‘static’ to assist in model fitting. We demonstrate how the method can be used to produce models of variable point sources and their host galaxies, enabling extraction of transient light curves and positions, and host galaxy morphology models and SEDs. The method has been applied to simulated supernova imaging at LSST-like resolutions, low-resolution ZTF imaging of tidal disruption events, and variable AGNs in the HSC-SSP transient survey. The automated initialization

procedures and the option to use prior-informed non-parametric galaxy models provide a high level of flexibility for various time-domain studies. The ability to carry out statistical sampling over source parameters in image space means that SCARLET2 can be used for careful quantification of uncertainties in source fluxes, positions, and host morphologies when studying systems of particular interest. We demonstrate that SCARLET2 can be used to confirm the spatial offsets of transients and their host galaxies for classification of nuclear and non-nuclear transients, and to identify populations of AGN ‘wandering’ away from their host galaxy nuclei.

This method will be most powerful when high cadence time-domain ground-based imaging from surveys like ZTF and LSST is jointly modeled with higher reso-

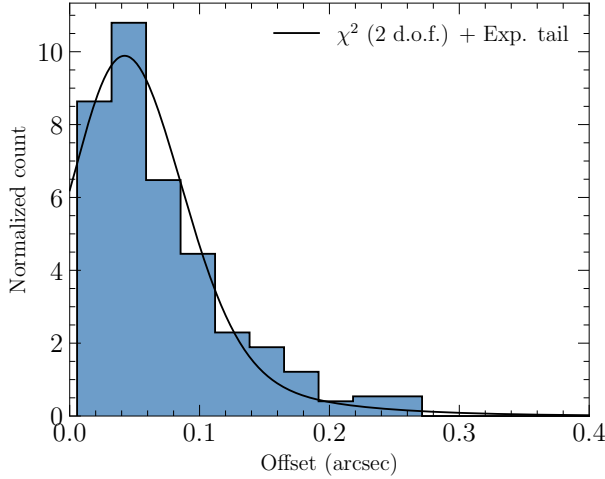


Figure 10: Histogram of host-AGN offsets for the COSMOS AGN population derived from SCARLET2 modeling of the full multi-epoch, multi-band HSC-SSP transient survey imaging dataset. The best-fit model of a mixture distribution of a Rayleigh distribution of $\sigma = 0.051''$ and an exponential tail with $\alpha = 14.2$ is shown in black.

lution space-based imaging from HST, *Euclid* (Racca et al., 2016), and the *Roman Space Telescope* (Akeson et al., 2019). The option for GPU acceleration means that image processing with SCARLET2 can be run at scale. We have made the SCARLET2 code available for the wider astrophysical community at <https://github.com/pmelchior/scarlet2>. Example jupyter notebooks for the methods described in each section are available at <https://github.com/charlotteaward/TimeDomainScarlet2>.

References

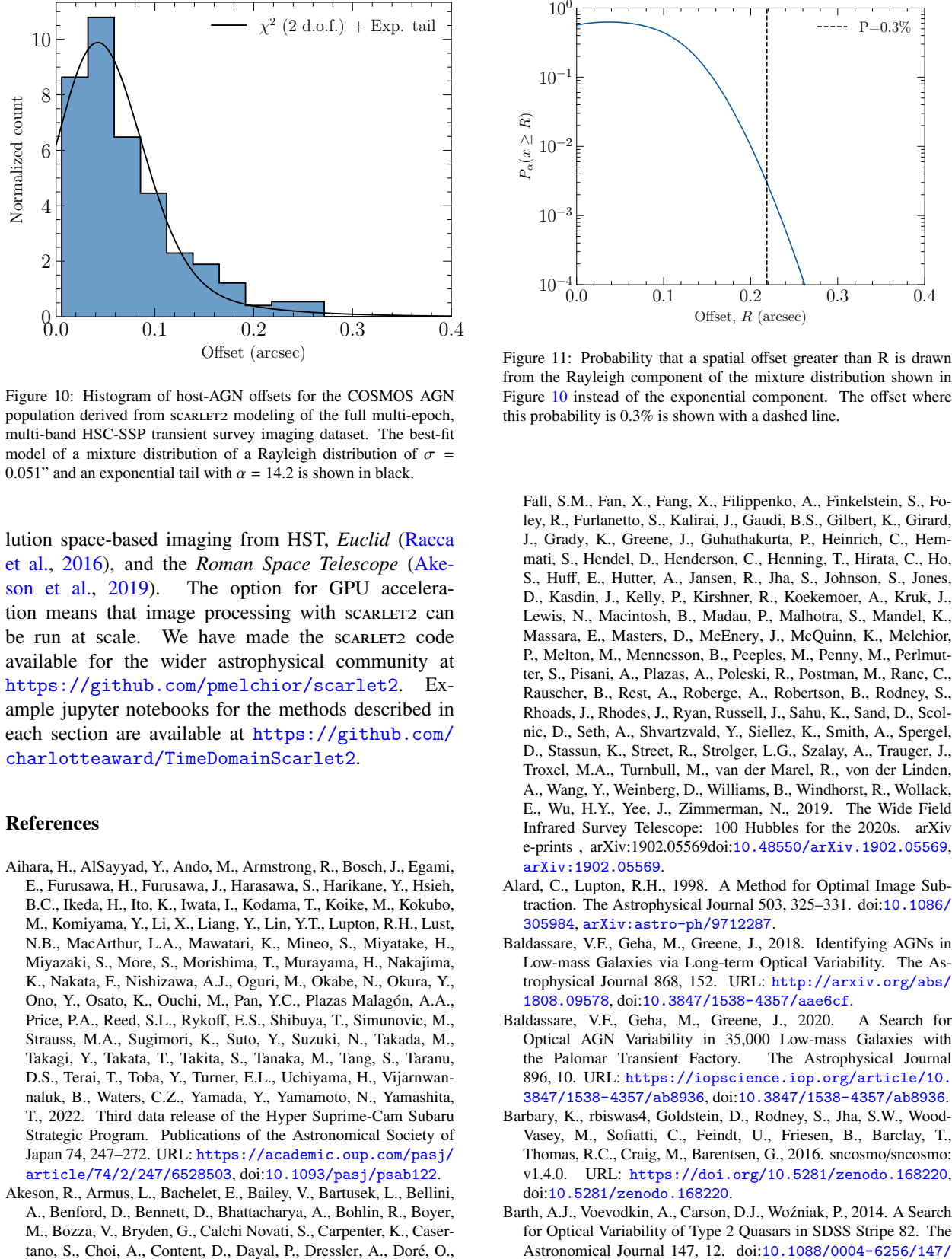


Figure 11: Probability that a spatial offset greater than R is drawn from the Rayleigh component of the mixture distribution shown in Figure 10 instead of the exponential component. The offset where this probability is 0.3% is shown with a dashed line.

Aihara, H., AlSayyad, Y., Ando, M., Armstrong, R., Bosch, J., Egami, E., Furusawa, H., Furusawa, J., Harasawa, S., Harikane, Y., Hsieh, B.C., Ikeda, H., Ito, K., Iwata, I., Kodama, T., Koike, M., Kokubo, M., Komiyama, Y., Li, X., Liang, Y., Lin, Y.T., Lupton, R.H., Lust, N.B., MacArthur, L.A., Mawatari, K., Mineo, S., Miyatake, H., Miyazaki, S., More, S., Morishima, T., Murayama, H., Nakajima, K., Nakata, F., Nishizawa, A.J., Oguri, M., Okabe, N., Okura, Y., Ono, Y., Osato, K., Ouchi, M., Pan, Y.C., Plazas Malagón, A.A., Price, P.A., Reed, S.L., Rykoff, E.S., Shibuya, T., Simunovic, M., Strauss, M.A., Sugimori, K., Suto, Y., Suzuki, N., Takada, M., Takagi, Y., Takata, T., Takita, S., Tanaka, M., Tang, S., Taranu, D.S., Terai, T., Toba, Y., Turner, E.L., Uchiyama, H., Vijarnwanaluk, B., Waters, C.Z., Yamada, Y., Yamamoto, N., Yamashita, T., 2022. Third data release of the Hyper Suprime-Cam Subaru Strategic Program. Publications of the Astronomical Society of Japan 74, 247–272. URL: <https://academic.oup.com/pasj/article/74/2/247/6528503>, doi:10.1093/pasj/psab122.

Akeson, R., Armus, L., Bachelet, E., Bailey, V., Bartusek, L., Bellini, A., Benford, D., Bennett, D., Bhattacharya, A., Bohlin, R., Boyer, M., Bozza, V., Bryden, G., Calchi Novati, S., Carpenter, K., Casertano, S., Choi, A., Content, D., Dayal, P., Dressler, A., Doré, O., Fall, S.M., Fan, X., Fang, X., Filippenko, A., Finkelstein, S., Foley, R., Furlanetto, S., Kalirai, J., Gaudi, B.S., Gilbert, K., Girard, J., Grady, K., Greene, J., Guhathakurta, P., Heinrich, C., Hemmati, S., Hendel, D., Henderson, C., Henning, T., Hirata, C., Ho, S., Huff, E., Hutter, A., Jansen, R., Jha, S., Johnson, S., Jones, D., Kasdin, J., Kelly, P., Kirshner, R., Koekemoer, A., Kruk, J., Lewis, N., Macintosh, B., Madau, P., Malhotra, S., Mandel, K., Massara, E., Masters, D., McEnery, J., McQuinn, K., Melchior, P., Melton, M., Mennesson, B., Peebles, M., Penny, M., Perlmutter, S., Pisani, A., Plazas, A., Poleski, R., Postman, M., Ranc, C., Rauscher, B., Rest, A., Roberge, A., Robertson, B., Rodney, S., Rhoads, J., Rhodes, J., Ryan, Russell, J., Sahu, K., Sand, D., Scolnic, D., Seth, A., Shvartzvald, Y., Siellez, K., Smith, A., Spergel, D., Stassun, K., Street, R., Strolger, L.G., Szalay, A., Trauger, J., Troxel, M.A., Turnbull, M., van der Marel, R., von der Linden, A., Wang, Y., Weinberg, D., Williams, B., Windhorst, R., Wollack, E., Wu, H.Y., Yee, J., Zimmerman, N., 2019. The Wide Field Infrared Survey Telescope: 100 Hubbles for the 2020s. arXiv e-prints , arXiv:1902.05569doi:10.48550/arXiv.1902.05569, arXiv:1902.05569.

Alard, C., Lupton, R.H., 1998. A Method for Optimal Image Subtraction. The Astrophysical Journal 503, 325–331. doi:10.1086/305984, arXiv:astro-ph/9712287.

Baldassare, V.F., Geha, M., Greene, J., 2018. Identifying AGNs in Low-mass Galaxies via Long-term Optical Variability. The Astrophysical Journal 868, 152. URL: <http://arxiv.org/abs/1808.09578>, doi:10.3847/1538-4357/aae6cf.

Baldassare, V.F., Geha, M., Greene, J., 2020. A Search for Optical AGN Variability in 35,000 Low-mass Galaxies with the Palomar Transient Factory. The Astrophysical Journal 896, 10. URL: <https://iopscience.iop.org/article/10.3847/1538-4357/ab8936>.

Barbary, K., rbiswas4, Goldstein, D., Rodney, S., Jha, S.W., Wood-Vasey, M., Sofiatti, C., Feindt, U., Friesen, B., Barclay, T., Thomas, R.C., Craig, M., Barentsen, G., 2016. sncosmo/sncosmo: v1.4.0. URL: <https://doi.org/10.5281/zenodo.168220>, doi:10.5281/zenodo.168220.

Barth, A.J., Voevodkin, A., Carson, D.J., Woźniak, P., 2014. A Search for Optical Variability of Type 2 Quasars in SDSS Stripe 82. The Astronomical Journal 147, 12. doi:10.1088/0004-6256/147/

1/12, arXiv:1310.0874.

Bellm, E.C., Kulkarni, S.R., Graham, M.J., Dekany, R., Smith, R.M., Riddle, R., Masci, F.J., Helou, G., Prince, T.A., Adams, S.M., Barbarino, C., Barlow, T., Bauer, J., Beck, R., Belicki, J., Biswas, R., Blagorodnova, N., Bodewits, D., Bolin, B., Brinnel, V., Brooke, T., Bue, B., Bulla, M., Burruzz, R., Cenko, S.B., Chang, C.K., Connolly, A., Coughlin, M., Cromer, J., Cunningham, V., De, K., Delacroix, A., Desai, V., Duev, D.A., Eadie, G., Farnham, T.L., Feeney, M., Feindt, U., Flynn, D., Franckowiak, A., Frederick, S., Fremling, C., Gal-Yam, A., Gezari, S., Giomi, M., Goldstein, D.A., Golkhou, V.Z., Goobar, A., Groom, S., Hacopians, E., Hale, D., Henning, J., Ho, A.Y.Q., Hover, D., Howell, J., Hung, T., Huppenkothen, D., Imel, D., Ip, W.H., Ivezic, Z., Jackson, E., Jones, L., Juric, M., Kasliwal, M.M., Kaspi, S., Kaye, S., Kelley, M.S.P., Kowalski, M., Kramer, E., Kupfer, T., Landry, W., Laher, R.R., Lee, C.D., Lin, H.W., Lin, Z.Y., Lunnan, R., Giomi, M., Mahabal, A., Mao, P., Miller, A.A., Monkewitz, S., Murphy, P., Ngeow, C.C., Nordin, J., Nugent, P., Ofek, E., Patterson, M.T., Penprase, B., Porter, M., Rauch, L., Rebbapragada, U., Reiley, D., Rigault, M., Rodriguez, H., Roestel, J.v., Rusholme, B., Santen, J.v., Schulze, S., Shupe, D.L., Singer, L.P., Soumagnac, M.T., Stein, R., Surace, J., Sollerman, J., Szkody, P., Taddia, F., Terek, S., Van Sistine, A., van Velzen, S., Vestrand, W.T., Walters, R., Ward, C., Ye, Q.Z., Yu, P.C., Yan, L., Zolkower, J., 2019. The Zwicky Transient Facility: System Overview, Performance, and First Results. *Publications of the Astronomical Society of the Pacific* 131, 018002. URL: <https://iopscience.iop.org/article/10.1088/1538-3873/aaecbe>, doi:10.1088/1538-3873/aaecbe.

Bellovary, J.M., Cleary, C.E., Munshi, F., Tremmel, M., Christensen, C.R., Brooks, A., Quinn, T.R., 2019. Multimessenger signatures of massive black holes in dwarf galaxies. *Monthly Notices of the Royal Astronomical Society* 482, 2913–2923. doi:10.1093/mnras/sty2842.

Bianco, F.B., Ivezic, Ž., Jones, R.L., Graham, M.L., Marshall, P., Saha, A., Strauss, M.A., Yoachim, P., Ribeiro, T., Anguita, T., Bauer, A.E., Bauer, F.E., Bellm, E.C., Blum, R.D., Brandt, W.N., Brough, S., Catelan, M., Clarkson, W.I., Connolly, A.J., Gawiser, E., Gizis, J.E., Hložek, R., Kaviraj, S., Liu, C.T., Lochner, M., Mahabal, A.A., Mandelbaum, R., McGehee, P., Neilsen, Eric H., J., Olsen, K.A.G., Peiris, H.V., Rhodes, J., Richards, G.T., Ridgway, S., Schwamb, M.E., Scolnic, D., Shemmer, O., Slater, C.T., Slosar, A., Smartt, S.J., Strader, J., Street, R., Trilling, D.E., Verma, A., Vivas, A.K., Wechsler, R.H., Willman, B., 2022. Optimization of the Observing Cadence for the Rubin Observatory Legacy Survey of Space and Time: A Pioneering Process of Community-focused Experimental Design. *The Astrophysical Journal Supplement Series* 258, 1. doi:10.3847/1538-4365/ac3e72, arXiv:2108.01683.

Bingham, E., Chen, J.P., Jankowiak, M., Obermeyer, F., Pradhan, N., Karlaftos, T., Singh, R., Szerlip, P.A., Horsfall, P., Goodman, N.D., 2019. Pyro: Deep universal probabilistic programming. *J. Mach. Learn. Res.* 20, 28:1–28:6. URL: <http://jmlr.org/papers/v20/18-403.html>.

Boquien, M., Burgarella, D., Roehlly, Y., Buat, V., Ciesla, L., Corre, D., Inoue, A.K., Salas, H., 2019. CIGALE: a python Code Investigating GALaxy Emission. *Astronomy & Astrophysics* 622, A103. doi:10.1051/0004-6361/201834156, arXiv:1811.03094.

Bosch, J., Armstrong, R., Bickerton, S., Furusawa, H., Ikeda, H., Koike, M., Lupton, R., Mineo, S., Price, P., Takata, T., Tanaka, M., Yasuda, N., AlSayyad, Y., Becker, A.C., Coulton, W., Coupon, J., Garmilla, J., Huang, S., Krughoff, K.S., Lang, D., Leauthaud, A., Lim, K.T., Lust, N.B., MacArthur, L.A., Mandelbaum, R., Miyatake, H., Miyazaki, S., Murata, R., More, S., Okura, Y., Owen, R., Swinbank, J.D., Strauss, M.A., Yamada, Y., Yamanoi, H., 2018. The Hyper Suprime-Cam software pipeline. *Publications of the Astronomical Society of Japan* 70. doi:10.1093/pasj/psx080.

Bradbury, J., Frostig, R., Hawkins, P., Johnson, M.J., Leary, C., Maclaurin, D., Necula, G., Paszke, A., VanderPlas, J., Wanderman-Milne, S., Zhang, Q., 2018. JAX: composable transformations of Python+NumPy programs. URL: <http://github.com/google/jax>.

Brightman, M., Ward, C., Stern, D., Mooley, K., De, K., Gezari, S., Van Velzen, S., Andreoni, I., Graham, M., Masci, F.J., Riddle, R., Zolkower, J., 2021. A Luminous X-Ray Transient in SDSS J143359.16+400636.0: A Likely Tidal Disruption Event. *The Astrophysical Journal* 909, 102. doi:10.3847/1538-4357/abde34.

Brout, D., Sako, M., Scolnic, D., Kessler, R., D'Andrea, C.B., Davis, T.M., Hinton, S.R., Kim, A.G., Lasker, J., Macaulay, E., Möller, A., Nichol, R.C., Smith, M., Sullivan, M., Wolf, R.C., Allam, S., Bassett, B.A., Brown, P., Castander, F.J., Childress, M., Foley, R.J., Galbany, L., Herner, K., Kasai, E., March, M., Morganson, E., Nugent, P., Pan, Y.C., Thomas, R.C., Tucker, B.E., Wester, W., Abbott, T.M.C., Annis, J., Avila, S., Bertin, E., Brooks, D., Burke, D.L., Carnero Rosell, A., Carrasco Kind, M., Carretero, J., Crocce, M., Cunha, C.E., da Costa, L.N., Davis, C., De Vicente, J., Desai, S., Diehl, H.T., Doel, P., Eifler, T.F., Flaugher, B., Fosalba, P., Frieman, J., García-Bellido, J., Gaztanaga, E., Gerdes, D.W., Goldstein, D.A., Gruen, D., Gruendl, R.A., Gschwend, J., Gutierrez, G., Hartley, W.G., Hollowood, D.L., Honscheid, K., James, D.J., Kuehn, K., Kuropatkin, N., Lahav, O., Li, T.S., Lima, M., Marshall, J.L., Martini, P., Miquel, R., Nord, B., Plazas, A.A., Roodman, A., Rykoff, E.S., Sanchez, E., Scarpine, V., Schindler, R., Schubnell, M., Serrano, S., Sevilla-Noarbe, I., Soares-Santos, M., Sobreira, F., Suchyta, E., Swanson, M.E.C., Tarle, G., Thomas, D., Tucker, D.L., Walker, A.R., Yanny, B., Zhang, Y., DES COLLABORATION, 2019. First Cosmology Results Using Type Ia Supernovae from the Dark Energy Survey: Photometric Pipeline and Light-curve Data Release. *The Astrophysical Journal* 874, 106. doi:10.3847/1538-4357/ab06c1, arXiv:1811.02378.

Burke, C.J., Liu, X., Shen, Y., Phadke, K.A., Yang, Q., Hartley, W.G., Harrison, I., Palmese, A., Guo, H., Zhang, K., Kron, R., Turner, D.J., Giles, P.A., Lidman, C., Chen, Y.C., Gruendl, R.A., Choi, A., Amon, A., Sheldon, E., Aguena, M., Allam, S., Andrade-Oliveira, F., Bacon, D., Bertin, E., Brooks, D., Rosell, A.C., Kind, M.C., Carretero, J., Conselice, C., Costanzi, M., da Costa, L.N., Pereira, M.E.S., Davis, T.M., De Vicente, J., Desai, S., Diehl, H.T., Everett, S., Ferrero, I., Flaugher, B., García-Bellido, J., Gaztanaga, E., Gruen, D., Gschwend, J., Gutierrez, G., Hinton, S.R., Hollowood, D.L., Honscheid, K., Hoyle, B., James, D.J., Kuehn, K., Maia, M.A.G., Marshall, J.L., Menanteau, F., Miquel, R., Morgan, R., Paz-Chinchón, F., Pieres, A., Malagón, A.A.P., Reil, K., Romer, A.K., Sanchez, E., Schubnell, M., Serrano, S., Sevilla-Noarbe, I., Smith, M., Suchyta, E., Tarle, G., Thomas, D., To, C., Varga, T.N., Wilkinson, R.D., 2022. Dwarf AGNs from Optical Variability for the Origins of Seeds (DAVOS): insights from the dark energy survey deep fields. *MNRAS* 516, 2736–2756. URL: <https://academic.oup.com/mnras/article/516/2/2736/6665940>, doi:10.1093/mnras/stac2262.

Burke, C.J., Liu, Y., Ward, C.A., Liu, X., Natarajan, P., Greene, J.E., 2024. DAVOS: Dwarf Active Galactic Nuclei from Variability for the Origins of Seeds: Properties of Variability-selected Active Galactic Nuclei in the COSMOS Field and Expectations for the Rubin Observatory. *The Astrophysical Journal* 971, 140. doi:10.3847/1538-4357/ad54ca, arXiv:2402.06882.

Burke, C.J., Shen, Y., Liu, X., Natarajan, P., Caplar, N., Bellovary, J.M., Wang, Z.F., 2023. Dwarf AGNs from variability for the origins of seeds (DAVOS): Intermediate-mass black hole demographics from optical synoptic surveys. *Monthly Notices of the Royal Astronomical Society* 518, 1880–1904. doi:10.1093/mnras/stac2478.

Butler, N.R., Bloom, J.S., 2011. Optimal Time-series Selection of Quasars. *The Astronomical Journal* 141, 93. doi:[10.1088/0004-6256/141/3/93](https://doi.org/10.1088/0004-6256/141/3/93), arXiv:[1008.3143](https://arxiv.org/abs/1008.3143).

De Cicco, D., Bauer, F.E., Paolillo, M., Cavaoti, S., Sánchez-Sáez, P., Brandt, W.N., Pignata, G., Vaccari, M., Radovich, M., 2021. A random forest-based selection of optically variable AGN in the VST-COSMOS field. *Astronomy & Astrophysics* 645, A103. doi:[10.1051/0004-6361/202039193](https://doi.org/10.1051/0004-6361/202039193), arXiv:[2011.08860](https://arxiv.org/abs/2011.08860).

Dekany, R., Smith, R.M., Riddle, R., Feeney, M., Porter, M., Hale, D., Zolkower, J., Belicki, J., Kaye, S., Henning, J., Walters, R., Cromer, J., Delacroix, A., Rodriguez, H., Reiley, D.J., Mao, P., Hover, D., Murphy, P., Burruss, R., Baker, J., Kowalski, M., Reif, K., Mueller, P., Bellm, E., Graham, M., Kulkarni, S.R., 2020. The Zwicky Transient Facility: Observing System. *Publications of the Astronomical Society of the Pacific* 132, 038001. doi:[10.1088/1538-3873/ab4ca2](https://doi.org/10.1088/1538-3873/ab4ca2).

Dey, A., Schlegel, D.J., Lang, D., Blum, R., Burleigh, K., Fan, X., Findlay, J.R., Finkbeiner, D., Herrera, D., Juneau, S., Landriau, M., Levi, M., McGreer, I., Meisner, A., Myers, A.D., Moustakas, J., Nugent, P., Patej, A., Schlafly, E.F., Walker, A.R., Valdes, F., Weaver, B.A., Yéche, C., Zou, H., Zhou, X., Abareshi, B., Abbott, T.M.C., Abolfathi, B., Aguilera, C., Alam, S., Allen, L., Alvarez, A., Annis, J., Ansarinejad, B., Aubert, M., Beechert, J., Bell, E.F., BenZvi, S.Y., Beutler, F., Bielby, R.M., Bolton, A.S., Briceño, C., Buckley-Geer, E.J., Butler, K., Calamida, A., Carlberg, R.G., Carter, P., Casas, R., Castander, F.J., Choi, Y., Comparat, J., Cukanovaite, E., Delubac, T., DeVries, K., Dey, S., Dhungana, G., Dickinson, M., Ding, Z., Donaldson, J.B., Duan, Y., Duckworth, C.J., Eftekharzadeh, S., Eisenstein, D.J., Etourneau, T., Fagrelius, P.A., Farihi, J., Fitzpatrick, M., Font-Ribera, A., Fulmer, L., Gänsicke, B.T., Gaztanaga, E., George, K., Gerdes, D.W., Gontcho, S.G.A., Gorgoni, C., Green, G., Guy, J., Harmer, D., Hernandez, M., Honscheid, K., Huang, L.W., James, D.J., Januzzi, B.T., Jiang, L., Joyce, R., Karcher, A., Karkar, S., Kehoe, R., Kneib, J.P., Kueter-Young, A., Lan, T.W., Lauer, T.R., Le Guillou, L., Le Van Suu, A., Lee, J.H., Lesser, M., Perreault Levasseur, L., Li, T.S., Mann, J.L., Marshall, R., Martínez-Vázquez, C.E., Martini, P., du Mas des Bourboux, H., McManus, S., Meier, T.G., Ménard, B., Metcalfe, N., Muñoz-Gutiérrez, A., Najita, J., Napier, K., Narayan, G., Newman, J.A., Nie, J., Nord, B., Norman, D.J., Olsen, K.A.G., Paat, A., Palanque-Delabrouille, N., Peng, X., Poppett, C.L., Poremba, M.R., Prakash, A., Rabinowitz, D., Raichoor, A., Rezaie, M., Robertson, A.N., Roe, N.A., Ross, A.J., Ross, N.P., Rudnick, G., Safonova, S., Saha, A., Sánchez, F.J., Savary, E., Schweiker, H., Scott, A., Seo, H.J., Shan, H., Silva, D.R., Slepian, Z., Soto, C., Sprayberry, D., Staten, R., Stillman, C.M., Stupak, R.J., Summers, D.L., Sien Tie, S., Tirado, H., Vargas-Magaña, M., Vivas, A.K., Wechsler, R.H., Williams, D., Yang, J., Yang, Q., Yapici, T., Zaritsky, D., Zenteno, A., Zhang, K., Zhang, T., Zhou, R., Zhou, Z., 2019. Overview of the DESI Legacy Imaging Surveys. *The Astronomical Journal* 157, 168. doi:[10.3847/1538-3881/ab089d](https://doi.org/10.3847/1538-3881/ab089d), arXiv:[1804.08657](https://arxiv.org/abs/1804.08657).

Di Matteo, T., Ni, Y., Chen, N., Croft, R., Bird, S., Pacucci, F., Ricarte, A., Tremmel, M., 2023. A vast population of wandering and merging IMBHs at cosmic noon. *Monthly Notices of the Royal Astronomical Society* 525, 1479–1497. URL: <https://academic.oup.com/mnras/article/525/1/1479/7243407>, doi:[10.1093/mnras/stad2198](https://doi.org/10.1093/mnras/stad2198).

Graham, M.J., Kulkarni, S.R., Bellm, E.C., Adams, S.M., Barbarino, C., Blagorodnova, N., Bodewits, D., Bolin, B., Brady, P.R., Cenko, S.B., Chang, C.K., Coughlin, M.W., Kishalay De, K., Eadie, G., Farnham, T.L., Feindt, U., Franckowiak, A., Fremling, C., Gezari, S., Ghosh, S., Goldstein, D.A., Golkhou, V.Z., Goobar, A., Ho, A.Y., Huppenkothen, D., Ivezić, Z., Jones, R.L., Juric, M., Kaplan, D.L., Kasliwal, M.M., Kelley, M.S., Kupfer, T., Lee, C.D., Lin, H.W., Lunnan, R., Mahabal, A.A., Miller, A.A., Ngeow, C.C., Nugent, P., Ofek, E.O., Prince, T.A., Rauch, L., Van Roestel, J., Schulze, S., Singer, L.P., Sollerman, J., Taddia, F., Yan, L., Ye, Q.Z., Yu, P.C., Barlow, T., Bauer, J., Beck, R., Belicki, J., Biswas, R., Brinnel, V., Brooke, T., Bue, B., Bulla, M., Burruss, R., Connolly, A., Cromer, J., Cunningham, V., Dekany, R., Delacroix, A., Desai, V., Duev, D.A., Feeney, M., Flynn, D., Frederick, S., Gal-Yam, A., Giomi, M., Groom, S., Hacopians, E., Hale, D., Helou, G., Henning, J., Hover, D., Hillenbrand, L.A., Howell, J., Hung, T., Imel, D., Ip, W.H., Jackson, E., Kaspi, S., Kaye, S., Kowalski, M., Kramer, E., Kuhn, M., Landry, W., Laher, R.R., Mao, P., Masci, F.J., Monkewitz, S., Murphy, P., Nordin, J., Patterson, M.T., Penprase, B., Porter, M., Rebbapragada, U., Reiley, D., Riddle, R., Rigault, M., Rodriguez, H., Rusholme, B., Van Santen, J., Shupe, D.L., Smith, R.M., Soumagnac, M.T., Stein, R., Surace, J., Szkody, P., Terek, S., Van Sistine, A., Van Velzen, S., Vestrand, W.T., Walters, R., Ward, C., Zhang, C., Zolkower, J., 2019. The zwicky transient facility: Science objectives. *Publications of the Astronomical Society of the Pacific* 131, 1–23. doi:[10.1088/1538-3873/ab0006](https://doi.org/10.1088/1538-3873/ab0006).

Holtzman, J.A., Marriner, J., Kessler, R., Sako, M., Dilday, B., Friedman, J.A., Schneider, D.P., Bassett, B., Becker, A., Cinabro, D., DeJongh, F., Depoy, D.L., Doi, M., Garnavich, P.M., Hogan, C.J., Jha, S., Konishi, K., Lampeitl, H., Marshall, J.L., McGinnis, D., Miknaitis, G., Nichol, R.C., Prieto, J.L., Riess, A.G., Richmond, M.W., Romani, R., Smith, M., Takanashi, N., Tokita, K., van der Heyden, K., Yasuda, N., Zheng, C., 2008. The Sloan Digital Sky Survey-II: Photometry and Supernova IA Light Curves from the 2005 Data. *The Astronomical Journal* 136, 2306–2320. doi:[10.1088/0004-6256/136/6/2306](https://doi.org/10.1088/0004-6256/136/6/2306), arXiv:[0908.4277](https://arxiv.org/abs/0908.4277).

Ivezic, Z., Axelrod, T., Brandt, W.N., Burke, D.L., Claver, C.F., Connolly, A., Cook, K.H., Gee, P., Gilmore, D.K., Jacoby, S.H., Jones, R.L., Kahn, S.M., Kantor, J.P., Krabbendam, V.V., Lupton, R.H., Monet, D.G., Pinto, P.A., Saha, A., Schalk, T.L., Schneider, D.P., Strauss, M.A., Stubbs, C.W., Sweeney, D., Szalay, A., Thaler, J.J., Tyson, J.A., LSST Collaboration, 2008. Large Synoptic Survey Telescope: From Science Drivers To Reference Design. *Serbian Astronomical Journal* 176, 1–13. doi:[10.2298/SAJ0876001I](https://doi.org/10.2298/SAJ0876001I).

Kidger, P., Garcia, C., 2021. Equinox: neural networks in JAX via callable PyTrees and filtered transformations. *Differentiable Programming workshop at Neural Information Processing Systems 2021*.

Lang, D., Hogg, D.W., Mykytyn, D., 2016. The Tractor: Probabilistic astronomical source detection and measurement. *Astrophysics Source Code Library*.

Lang, D., Hogg, D.W., Schlegel, D.J., 2016. WISE Photometry for 400 Million SDSS Sources. *The Astronomical Journal* 151, 36. doi:[10.3847/0004-6256/151/2/36](https://doi.org/10.3847/0004-6256/151/2/36), arXiv:[1410.7397](https://arxiv.org/abs/1410.7397).

Lin, D., Strader, J., Carrasco, E.R., Page, D., Romanowsky, A.J., Homan, J., Irwin, J.A., Remillard, R.A., Godet, O., Webb, N.A., Baumgardt, H., Wijnands, R., Barret, D., Duc, P.A., Brodie, J.P., Gwyn, S.D.J., 2018. A luminous X-ray outburst from an intermediate-mass black hole in an off-centre star cluster. *Nature Astronomy* 2, 656–661. doi:[10.1038/s41550-018-0493-1](https://doi.org/10.1038/s41550-018-0493-1).

MacLeod, C.L., Brooks, K., Ivezić, Ž., Kochanek, C.S., Gibson, R., Meisner, A., Kozłowski, S., Sesar, B., Becker, A.C., de Vries, W.H., 2011. Quasar Selection Based on Photometric Variability. *The Astrophysical Journal* 728, 26. doi:[10.1088/0004-637X/728/1/26](https://doi.org/10.1088/0004-637X/728/1/26), arXiv:[1009.2081](https://arxiv.org/abs/1009.2081).

Masci, F.J., Laher, R.R., Rusholme, B., Shupe, D.L., Groom, S., Surace, J., Jackson, E., Monkewitz, S., Beck, R., Flynn, D., Terek, S., Landry, W., Hacopians, E., Desai, V., Howell, J., Brooke, T., Imel, D., Wachter, S., Ye, Q.Z., Lin, H.W., Cenko, S.B., Cunningham, V., Rebbapragada, U., Bue, B., Miller, A.A., Mahabal, A., Bellm, E.C., Patterson, M.T.,

Jurić, M., Golkhou, V.Z., Ofek, E.O., Walters, R., Graham, M., Kasliwal, M.M., Dekany, R.G., Kupfer, T., Burdge, K., Cannella, C.B., Barlow, T., Sistine, A.V., Giomi, M., Fremling, C., Blagorodnova, N., Levitan, D., Riddle, R., Smith, R.M., Helou, G., Prince, T.A., Kulkarni, S.R., 2019. The Zwicky Transient Facility: Data Processing, Products, and Archive. Publications of the Astronomical Society of the Pacific 131, 018003. URL: <https://iopscience.iop.org/article/10.1088/1538-3873/aae8ac>, doi:10.1088/1538-3873/aae8ac.

Melchior, P., Joseph, R., Sanchez, J., MacCrann, N., Gruen, D., 2021. The challenge of blending in large sky surveys. *Nature Reviews Physics* 3, 712–718. URL: <https://www.nature.com/articles/s42254-021-00353-y>, doi:10.1038/s42254-021-00353-y.

Melchior, P., Moolekamp, F., Jerdee, M., Armstrong, R., Sun, A.L., Bosch, J., Lupton, R., 2018. scarlet: Source separation in multi-band images by Constrained Matrix Factorization. *Astronomy and Computing* 24, 129–142. URL: <https://linkinghub.elsevier.com/retrieve/pii/S2213133718300301>, doi:10.1016/j.ascom.2018.07.001.

Nugent, A.E., Fong, W.F., Dong, Y., Leja, J., Berger, E., Zevin, M., Chornock, R., Cobb, B.E., Kelley, L.Z., Kilpatrick, C.D., Levan, A., Margutti, R., Paterson, K., Perley, D., Escoril, A.R., Smith, N., Tanvir, N., 2022. Short GRB Host Galaxies. II. A Legacy Sample of Redshifts, Stellar Population Properties, and Implications for Their Neutron Star Merger Origins. *The Astrophysical Journal* 940, 57. doi:10.3847/1538-4357/ac91d1, [arXiv:2206.01764](https://arxiv.org/abs/2206.01764).

Pacucci, F., Loeb, A., Mezcua, M., Martin-Navarro, I., 2018. Glimmering in the dark: Modeling the low-mass end of the $m - \sigma$ relation and of the quasar luminosity function. *The Astrophysical Journal* 864, L6. doi:10.3847/2041-8213/aad8b2.

Palanque-Delabrouille, N., Yèche, C., Myers, A.D., Petitjean, P., Ross, N.P., Sheldon, E., Aubourg, E., Delubac, T., Le Goff, J.M., Pâris, I., Rich, J., Dawson, K.S., Schneider, D.P., Weaver, B.A., 2011. Variability selected high-redshift quasars on SDSS Stripe 82. *Astronomy & Astrophysics* 530, A122. doi:10.1051/0004-6361/201016254, [arXiv:1012.2391](https://arxiv.org/abs/1012.2391).

Phan, D., Pradhan, N., Jankowiak, M., 2019. Composable effects for flexible and accelerated probabilistic programming in numpyro. *arXiv preprint arXiv:1912.11554*.

Racca, G.D., Laureijs, R., Stagnaro, L., Salvignol, J.C., Lorenzo Alvarez, J., Saavedra Criado, G., Gaspar Venancio, L., Short, A., Strada, P., Bönke, T., Colombo, C., Calvi, A., Maiorano, E., Pierantoni, O., Prezelus, S., Rosato, P., Pinel, J., Rozemeijer, H., Lesna, V., Musi, P., Sias, M., Anselmi, A., Cazaubiel, V., Vaillon, L., Mellier, Y., Amiaux, J., Berthé, M., Sauvage, M., Azzollini, R., Cörper, M., Pottinger, S., Jahnke, K., Ealet, A., Maciaszek, T., Pasian, F., Zacchei, A., Scaramella, R., Hoar, J., Kohley, R., Vavrek, R., Rudolph, A., Schmidt, M., 2016. The euclid mission design, in: MacEwen, H.A., Fazio, G.C., Lystrup, M., Batalha, N., Siegler, N., Tong, E.C. (Eds.), *Space Telescopes and Instrumentation 2016: Optical, Infrared, and Millimeter Wave, SPIE*. URL: <http://dx.doi.org/10.1117/12.2230762>, doi:10.1117/12.2230762.

Ricarte, A., Tremmel, M., Natarajan, P., Quinn, T., 2021. Unveiling the Population of Wandering Black Holes via Electromagnetic Signatures. *The Astrophysical Journal Letters* 916, L18. URL: <https://iopscience.iop.org/article/10.3847/2041-8213/ac1170>, doi:10.3847/2041-8213/ac1170.

Rigault, M., 2018. ztfquery, a python tool to access ZTF data. URL: <https://doi.org/10.5281/zenodo.1345222>, doi:10.5281/zenodo.1345222.

Rowe, B.T.P., Jarvis, M., Mandelbaum, R., Bernstein, G.M., Bosch, J., Simet, M., Meyers, J.E., Kacprzak, T., Nakajima, R., Zuntz, J., Miyatake, H., Dietrich, J.P., Armstrong, R., Melchior, P., Gill, M.S.S., 2015. GALSIM: The modular galaxy image simulation toolkit. *Astronomy and Computing* 10, 121–150. doi:10.1016/j.ascom.2015.02.002, [arXiv:1407.7676](https://arxiv.org/abs/1407.7676).

Sampson, M., Melchior, P., Ward, C., Birmingham, S., 2024. Score-matching neural networks for improved multi-band source separation. *Astronomy and Computing* 49, 100875. URL: <https://www.sciencedirect.com/science/article/pii/S2213133724000908>, doi:10.1016/j.ascom.2024.100875, [arXiv:2401.07313](https://arxiv.org/abs/2401.07313).

Savic, D.V., Jankov, I., Yu, W., Petrecca, V., Temple, M.J., Ni, Q., Shirley, R., Kovačević, A.B., Nikolić, M., Ilić, D., Popović, L.Č., Paolillo, M., Panda, S., Ćiprijanović, A., Richards, G.T., 2023. The LSST AGN Data Challenge: Selection Methods. *The Astrophysical Journal* 953, 138. doi:10.3847/1538-4357/ace31a, [arXiv:2307.04072](https://arxiv.org/abs/2307.04072).

Sesar, B., Ivezić, Ž., Lupton, R.H., Jurić, M., Gunn, J.E., Knapp, G.R., DeLee, N., Smith, J.A., Miknaitis, G., Lin, H., Tucker, D., Doi, M., Tanaka, M., Fukugita, M., Holtzman, J., Kent, S., Yanny, B., Schlegel, D., Finkbeiner, D., Padmanabhan, N., Rockosi, C.M., Bond, N., Lee, B., Stoughton, C., Jester, S., Harris, H., Harding, P., Brinkmann, J., Schneider, D.P., York, D., Richmond, M.W., Vanden Berk, D., 2007. Exploring the Variable Sky with the Sloan Digital Sky Survey. *The Astronomical Journal* 134, 2236–2251. doi:10.1088/521819, [arXiv:0704.0655](https://arxiv.org/abs/0704.0655).

Stone, C.J., Courteau, S., Cuillandre, J.C., Hezaveh, Y., Perreault-Levasseur, L., Arora, N., 2023. *iscp;astrophot;scp*: fitting everything everywhere all at once in astronomical images. *Monthly Notices of the Royal Astronomical Society* 525, 6377–6393. doi:10.1093/mnras/stad2477.

van Velzen, S., Gezari, S., Hammerstein, E., Roth, N., Frederick, S., Ward, C., Hung, T., Cenko, S.B., Stein, R., Perley, D.A., Taggart, K., Foley, R.J., Sollerman, J., Blagorodnova, N., Andreoni, I., Bellm, E.C., Brinnel, V., De, K., Dekany, R., Feeney, M., Fremling, C., Giomi, M., Golkhou, V.Z., Graham, M.J., Ho, A.Y.Q., Kasliwal, M.M., Kilpatrick, C.D., Kulkarni, S.R., Kupfer, T., Laher, R.R., Mahabal, A., Masci, F.J., Miller, A.A., Nordin, J., Riddle, R., Rusholme, B., Santen, J.V., Sharma, Y., Shupe, D.L., Soumagnac, M.T., 2021. Seventeen Tidal Disruption Events from the First Half of ZTF Survey Observations: Entering a New Era of Population Studies. *The Astrophysical Journal* 908, 4. URL: <https://iopscience.iop.org/article/10.3847/1538-4357/abc258>, doi:10.3847/1538-4357/abc258.

Ward, C., Gezari, S., Frederick, S., Hammerstein, E., Nugent, P., van Velzen, S., Drake, A., García-Pérez, A., Oyoo, I., Bellm, E.C., Duev, D.A., Graham, M.J., Kasliwal, M.M., Kaye, S., Mahabal, A.A., Masci, F.J., Rusholme, B., Soumagnac, M.T., Yan, L., 2021. AGNs on the Move: A Search for Off-nuclear AGNs from Recoiling Supermassive Black Holes and Ongoing Galaxy Mergers with the Zwicky Transient Facility. *The Astrophysical Journal* 913, 102. URL: <https://iopscience.iop.org/article/10.3847/1538-4357/abf246>, doi:10.3847/1538-4357/abf246.

Ward, C., Gezari, S., Nugent, P., Bellm, E.C., Dekany, R., Drake, A., Duev, D.A., Graham, M.J., Kasliwal, M.M., Kool, E.C., Masci, F.J., Riddle, R.L., 2022. Variability-selected Intermediate-mass Black Hole Candidates in Dwarf Galaxies from ZTF and WISE. *The Astrophysical Journal* 936, 104. URL: <https://iopscience.iop.org/article/10.3847/1538-4357/ac8666>, doi:10.3847/1538-4357/ac8666.

Yasuda, N., Tanaka, M., Tominaga, N., Jiang, J.a., Moriya, T.J., Morokuma, T., Suzuki, N., Takahashi, I., Yamaguchi, M.S., Maeda, K., Sako, M., Ikeda, S., Kimura, A., Morii, M., Ueda, N., Yoshida, N., Lee, C.H., Suyu, S.H., Komiyama, Y., Regnault, N., Rubin, D., 2019. The Hyper Suprime-Cam SSP transient survey in COSMOS: Overview. *Publications of the Astronomical Society of Japan* 71.

URL: <https://academic.oup.com/pasj/article/doi/10.1093/pasj/psz050/5506540>, doi:10.1093/pasj/psz050.
Zhong, Y., Inoue, A.K., Yamanaka, S., Yamada, T., 2022. A Morphological Study of Galaxies Hosting Optical Variability-selected AGNs in the COSMOS Field. *The Astrophysical Journal* 925, 157. doi:10.3847/1538-4357/ac3edb.